Journal of Materials Chemistry A

PAPER

View Article Online
View Journal | View Issue



Cite this: J. Mater. Chem. A, 2019, 7, 1810

# Glowing stereocomplex biopolymers are generating power: polylactide/carbon quantum dot hybrid nanofibers with high piezoresponse and multicolor luminescence†

Yali Xu,‡[a] Long Jin,‡[a] Xuebing He,[a] Xi Huang,[a] Meilin Xie,[a] Chuanfeng Wang,[a] Chaoliang Zhang,[c] Weiqing Yang,*[a] Fanbin Meng*[a] and Jun Lu §*[ab]

We report the design and fabrication of novel biodegradable hybrid polymeric nanofibers with the combined advantages of high shear piezoelectricity, multicolor photoluminescence and simultaneously improved heat resistance. The multifunctional flexible nanofibers, with uniform diameters and smooth surfaces, were fabricated through the electrospinning of poly(D-lactide) (PDLA)/poly(L-lactic acid) (PLLA)/carbon quantum dots (CQDs) with dichloromethane and alcohol as the mixed spinning solvent. The electrospinning at a high voltage enhanced the orientation and formation of stereocomplexed polylactide crystals, and at the same time remarkably suppressed the growth of homocrystallites in the ternary composite nanofibers. With the amplitude and/or frequency increase of stimulated dynamic loads, the electrical outputs of the stereocomplex PDLA/PLLA/CQD nanofibers increased, and the maximum open-circuit voltage and short-circuit current output density achieved were 74.2 V cm$^{-3}$ and 4.9 μA cm$^{-3}$, respectively. Also, the stereocomplexed nanofiber based nanogenerator, during continuous operation of electromechanical conversion, demonstrated good stability and durability as a power source to operate LEDs, and no electrical output decay was observed for more than 10 000 consecutive working cycles. Moreover, the electrospun hybridized nanofibers emitted different fluorescence colors under laser excitation at different wavelengths. The as-developed ecologically friendly bionanofibers may diversify niche applications in future transient electronics and implantable medical devices as self-powered bio-sensors, bio-piezoelectric nanogenerators, and so on.

Received 4th September 2018
Accepted 12th December 2018

DOI: 10.1039/c8ta08593e

rsc.li/materials-a



## Introduction

Energy harvesting through sustainable pathways has attracted wide interest in transforming the prevalent and otherwise wasted environmental energy into electrical power.[1–6] Diversified energy scavenging technologies have been developed *via* a variety of transduction mechanisms, including electromagnetic, electrostatic, piezoelectric and triboelectric processes.[1–6] Among the current available techniques, piezoelectric nanogenerators (PNGs) show more advantages in capturing kinetic mechanical energy with variable amplitudes and frequencies.[7,8] In particular, the PNGs utilizing sustainable piezopolymers from renewable resources, have a smaller ecological footprint, and are highly desired for the realization of a sustainable society.[1,9,10]

Piezoelectric polymers, with a non-centrosymmetric arrangement of atoms and molecules achieved by mechanical or electrical treatments, are categorized into two classes in terms of their operating principles and properties.[11,12] Class I polymers are those poled by a high electrical field to realize their piezoelectricity, and typically show a symmetry of $C_{\infty v}$, such as poly(vinylidene fluoride) and odd nylons.[11,12] Class II materials consist of uniaxially oriented chiral molecules, macroscopically aligned by mechanical stretching or a magnetic field, and are with the symmetry of $D_{\infty}$, such as polyesters with chiral repeat units.[11,12] Most of the optically active natural and synthetic biopolymers, including cellulose, collagen, polypeptides, poly(lactic acid) (PLA), and so on, are class II materials, and exhibit shear piezoelectricity, *i.e.* a coupling between uniaxial polarization and shear force or strain.[13–27] Although chiral

[a]Key Laboratory of Advanced Technologies of Materials, Ministry of Education, School of Materials Science and Engineering, Southwest Jiaotong University, Chengdu 610031, Sichuan, China. E-mail: junluprc@hotmail.com; wqyang@swjtu.edu.cn; mengfanbin_wing@126.com

[b]State Key Laboratory of Polymer Materials Engineering, Sichuan University, Chengdu 610065, Sichuan, China

[c]State Key Laboratory of Oral Diseases, West China Hospital of Stomatology, Sichuan University, Chengdu 610041, Sichuan, China

† Electronic supplementary information (ESI) available. See DOI: 10.1039/c8ta08593e

‡ These authors contributed equally to this work.

§ Other names used are Jun Lv and Jun Lyu.

biopiezopolymers have demonstrated such unique features as non-poling treatment, non-pyroelectricity, and depolarization resistance in bioelectronic devices, their piezoresponses are generally smaller than those of poled piezopolymers.[9,10,12,28] Therefore, recent advances in biopolymer based PNGs focus on boosting power generation and conversion efficiency.[5,9,10,12,28] Moreover, major challenges still lie in the design and fabrication of environmentally friendly hybridized biopolymers for the realization of multifunctional bio-PNGs with simultaneously improved combinational properties.[28–31]

PLA is a renewably sourced and commercially available biopolyester, commonly made from starch-rich crops such as maize, and is one of the most promising green alternatives to petrochemical-derived polymers.[1,32] According to the chirality of lactide monomers (L-, D-, or *meso*-), it is categorized into semi-crystalline PLLA and PDLA, and amorphous PDLLA.[33,34] The shear piezoresponse of optically active chiral PLA originates from the internal rotation of polar radicals associated with an asymmetric carbon atom, and the sign of its piezo-constant depends on the chirality of the asymmetric carbon atoms.[35–37] Also, the magnitude of the shear piezoelectric signal is linearly proportional to the orientation degree of molecular chains and/or crystallites.[35–37] Therefore, a few techniques have been developed to manufacture optically pure PLLA based films and fibers with increased orientation and crystallinity, for the purpose of achieving a relatively high shear piezoelectricity of the polymer, including electrospinning, magnetic field assisted drawing, and solid-state extrusion.[29,30,36–39] Among these, the simple and versatile electrospinning technique has demonstrated decisive advantages in the preparation of continuous and uniform PLLA nanofibers which have larger piezoelectric strain constants than their film counterparts.[29,30,36,37] For electrospinning, several parameters, such as solution concentration, solution feed rate, voltage, needle movement, and collection method, have a direct impact on the physical and mechanical properties of the products, and can be combined together to control the macro/microscopic orientation of the electrospun PLLA nanofibers.[36,40–42]

Stereocomplexation (sc) happens when D- and L-poly(lactic acid)s are melt or solution blended in equal proportions, mainly stemming from the strong C═O···$H_3$C interaction between the isomers.[43–48] The crystal structures and physical properties of sc PLA are distinct from the parent polymers, and sc formation has been proved to be an effective approach to enhance the thermal and mechanical properties of the polymer.[43–48] For example, the melting point of sc PLA crystallites is about 50 °C higher than that of homocrystals.[43–48] Also, sc-PLA demonstrates higher biocompatibility than optically pure polylactides, and has attracted particular interest due mainly to its potential as a matrix for biomedical purposes.[43–48] Unfortunately, D- and L-poly(lactic acid)s exhibit opposite signs of the piezoelectric constant.[35–37] Hence, the electrospinning technique, which enables the formation of stereocomplexes in electrospun blend fibers that follow one-dimensional growth, is expected to improve the piezoelectricity of a PLLA/PDLA mixture. Although the electrospinning of stereocomplex PLA nanofibers has been carried out,[43] to the best of our knowledge, no investigation was conducted on the piezoresponse of the sc bionanofibers as well as on integrating them with bio-PNGs for energy harvesting.

Carbon quantum dots (CQDs), a rising star of carbon nanomaterials, have garnered much interest as potential competitors to conventional semiconductor QDs, by virtue of their low toxicity, environmental friendliness, biocompatibility, adjustable luminescence range, low cost and simple synthetic routes.[49–54] CQDs are quasi-spherical nanoparticles, usually less than 10 nm in diameter, and can be amorphous or nanocrystalline with $sp^2$ carbon clusters.[49–54] Being considered as the next big "small" thing, CQDs have demonstrated enormous potential in bio-imaging, bio-sensing, theranostics, optoelectronics, and energy storage/conversion, though the research is still at an early stage.[49–54]

In this work, we report for the first time the electrospinning of stereocomplexed PDLA/PLLA/CQD based hybrid nanofibers, their photoluminescent properties, and their mechanical-to-electrical conversion *via* a direct piezoelectric response. The high voltage electrospinning significantly enhanced the orientation and growth of sc PLA crystallites in the ternary nanofibers, and enabled their high piezoresponse under mechanical stress. Also, the CQD hybridized nanofibers demonstrated an interesting multicolor fluorescence effect under light excitation at different wavelengths. Being assembled as a PNG, the electrospun stereocomplex bionanofibers could harvest from its working environment the dynamic mechanical energy with various amplitudes and/or frequencies, and the maximum open-circuit voltage and short-circuit current output density achieved were 74.2 V $cm^{-3}$ and 4.9 μA $cm^{-3}$, respectively. As a power source to operate LEDs, the stereocomplexed bio-PNG showed good stability and durability, and no decay in electrical output was observed for ≈10 000 continuous working cycles.

## Experimental part

PLLA and PDLA both have an intrinsic viscosity of 1.0–1.5 dl $g^{-1}$ and a weight-average molecular weight of 100 000 g $mol^{-1}$, and were purchased from Dai Gang Biological Engineering Co., Ltd, Jinan, China. CQDs were supplied by Newcastle New Materials Co., Ltd, Nanjing, China. As revealed by transmission electron microscopy (TEM), the original CQDs range from 3 to 7 nm in size (Fig. S1a–d, ESI†). Further TEM observations on PDLA/PLLA/CQDs showed that the CQDs intrinsically tended to aggregate on the nanoscale in the polymer matrix, and the size of the CQD aggregates increased with the increase of CQD loading (Fig. S1e and f, ESI†). The CQD aggregates range from 3–9 nm and 3–13 nm in size, respectively, for the PDLA/PLLA/CQDs with 1 wt% and 2 wt% CQD concentrations (Fig. S1e and f, ESI†). Analytical grade dichloromethane and alcohol were both provided by Kelong Chemical Co., Ltd, Chengdu, China, and were used as received.

A schematic illustration of the manufacturing process for an electrospun PDLA/PLLA/CQD nanofibrous film is shown in Fig. 1. Blended PLLA and PDLA was first dissolved in the mixed solvent of dichloromethane and alcohol (3 : 1, v/v) at 25 °C for 2 h to generate a transparent solution with a concentration of 120 mg $ml^{-1}$, and then CQDs were added with magnetic stirring for an additional 2 h. Afterwards, the well mixed

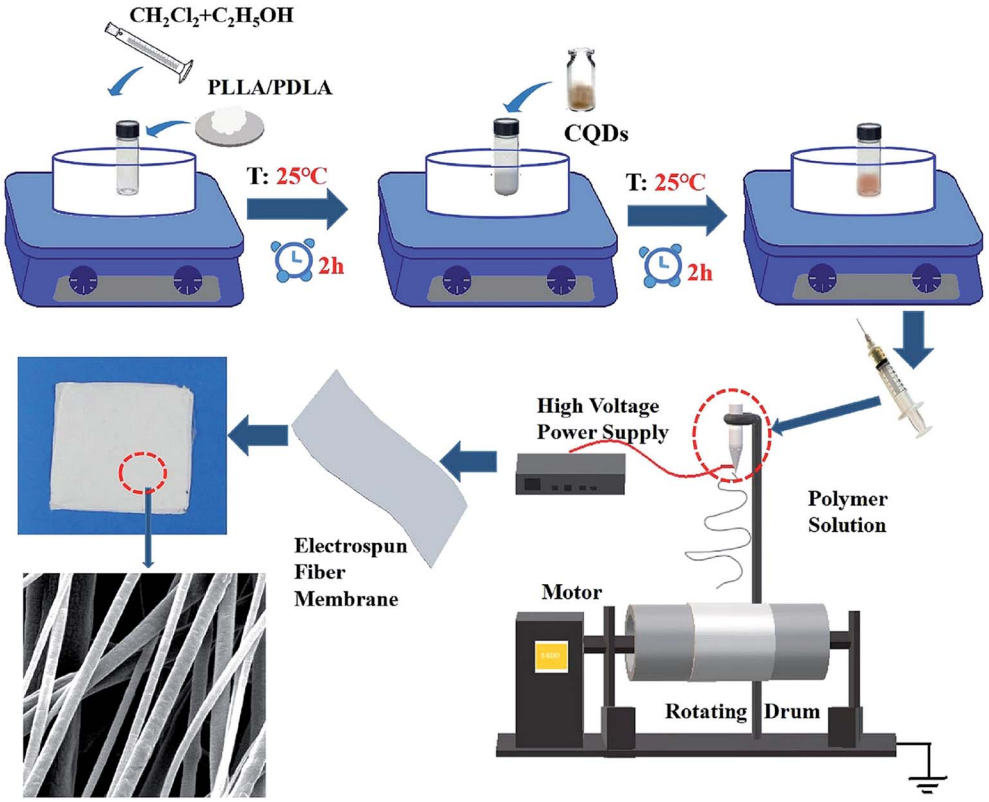


Fig. 1 Schematic diagram illustrating the manufacturing process of an electrospun PDLA/PLLA/CQD nanofibrous film.

electrospinning solution was poured into a 10 ml syringe connected to a spinneret with an inner diameter of 0.7 mm. A positive high-voltage supply was used to supply the voltage in a range of 0–30 kV. Herein, a 12 kV voltage was used during electrospinning, and the outflow rate was set to 20 microliters per minute. A rotating drum was used to collect the ejected fibers. The stepping speed, step displacement and rotating speed of the receiving device were set to 8 mm $s^{-1}$, 60 mm and 1400 rpm, respectively. After electrospinning, the nanofiber membranes were scraped off the drum and stored in a sealed bag. For comparison, PDLA/PLLA/CQD nanofibers were also fabricated with different PDLA/PLLA ratios, electrospinning voltages and rotating drum speeds. The electrospun bionanofibers with various compounding ratios, were coded as PDLA/PLLA/CQD *x*/*y*/*z*, where *x*, *y* and *z* represent the weight percentages of PDLA, PLLA and CQDs, respectively.

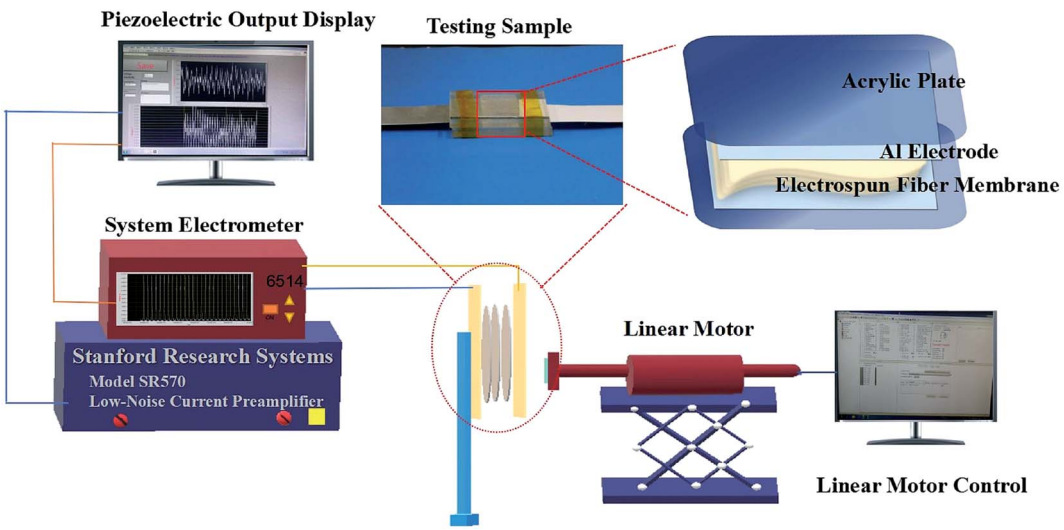


Fig. 2 Schematic representation of the impact measurement system for concurrently collecting the generated electrical potential and current outputs, and the structural assembly of test samples.

 

TEM observations were performed with a JEOL JEM-2100F apparatus. Laser scanning confocal microscope (LSCM) observations were conducted with a Nikon A1R+ apparatus. Photoluminescence (PL) spectra were obtained at room temperature using a FLS980 spectrometer (Edinburgh Instruments) with a 450 W xenon lamp. On the basis of the PL spectra, a 1931 CIE (Commission Internationale de L'Eclairage) system was used to calculate the chromaticity coordinates. The morphology of the resulting nanofiber membranes was examined with scanning electron microscopy (SEM) using a JSM-6330F apparatus after gold coating. Differential scanning calorimetry (DSC) measurements were carried out at atmospheric pressure with a TA-Q20 instrument. The weight of each sample was around 5 mg. Under a $N_2$ atmosphere, the samples were heated from 0 to 250 °C at a rate of 10 °C $min^{-1}$ and then cooled down to 40 °C.

After being integrated as nanogenerators, periodic impact tests were performed on homemade devices to evaluate the energy harvesting performance of the electrospun nanofibrous films. A schematic drawing of the measurement system, as well as the structural assembly of the test PNG samples, is shown in Fig. 2. To eliminate the interference of triboelectric charges, the PNGs were encapsulated within acrylic resin, the same material used in the impact head. A NTIAG HS01-37 × 166 linear motor was used as the impact source, and the generated open-circuit voltage and short-circuit current were simultaneously collected with a Keithley 6514 system electrometer and a Stanford Research SR570 low-noise current preamplifier, respectively.

## Results and discussion

Fig. 3a–i show the LSCM images of the electrospun PDLA/PLLA/CQD nanofibers with various CQD concentrations, under different excitation wavelengths of light. As can be seen clearly, no fluorescence response was observed for the $PDLA_{50}/PLLA_{50}$ nanofibers, whereas the hybrid PDLA/PLLA/CQD bionanofibers produced different colors under variable light excitations, emitting blue, green and red light fluorescence under the excitation with purple, blue and red light, respectively. Thus, the successful incorporation of CQDs during electrospinning endowed the hybridized biopolymeric nanofibers with the desirable excitation-light dependent multicolor luminescence that has a direct influence in extending their applications. Fig. 3j shows the typical PL emission spectra of the electrospun PDLA/PLLA/CQD based nanofibers, with 1 wt% and 2 wt% CQD loadings, respectively. As already revealed by TEM (Fig. S1, ESI†), the CQDs tend to aggregate in the PDLA/PLLA matrix. The CQD aggregates range from 3–9 nm and 3–13 nm in size, respectively, for the $PDLA_{49.5}/PLLA_{49.5}/CQD_1$ and $PDLA_{49}/PLLA_{49}/CQD_2$ based composites (Fig. S1, ESI†). This further resulted in different photoluminescence response results for

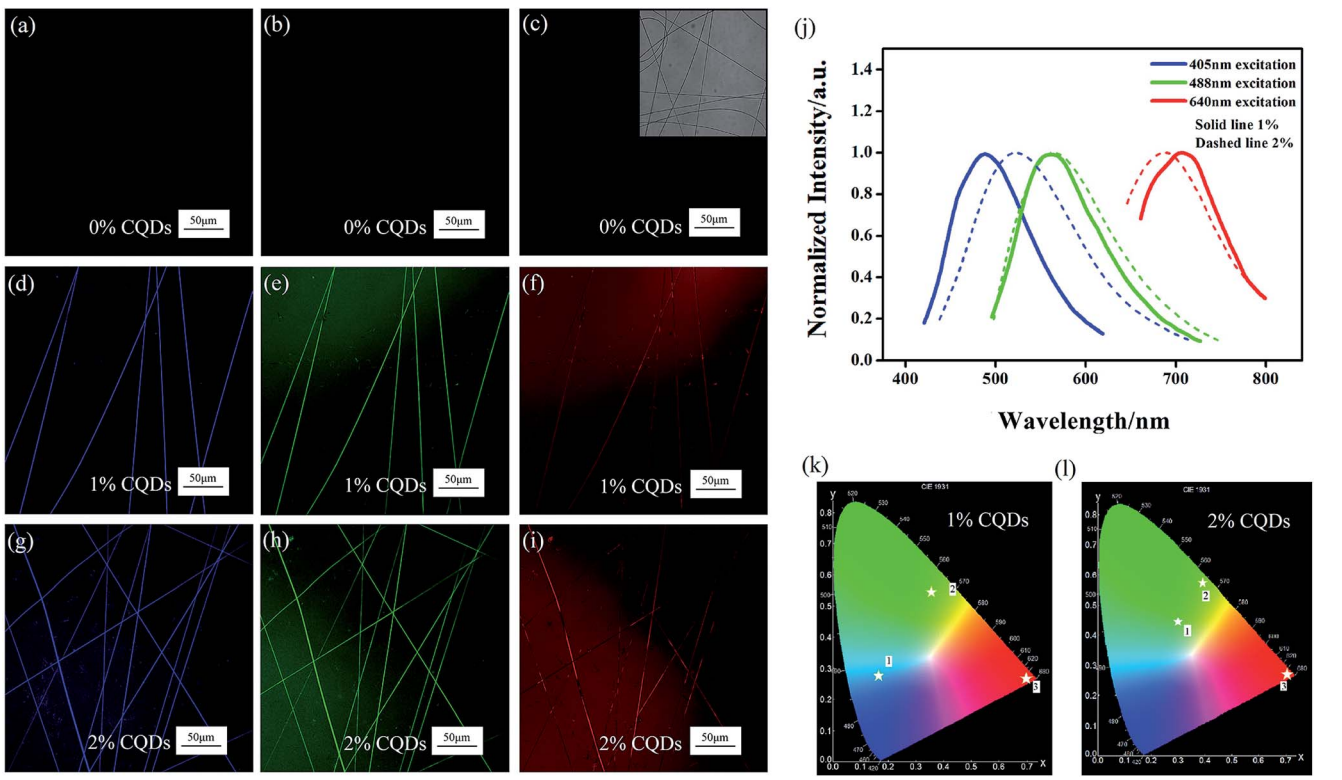


Fig. 3 Laser scanning confocal microscope images of the electrospun PDLA/PLLA/CQD nanofibers with various CQD concentrations, observed at purple (a, d and g), blue (b, e and h) and red (c, f and i) light excitations, respectively, and typical PL spectra (j) and CIE diagrams (k and l) of the PDLA/PLLA/CQD mixtures, under 405, 488 and 640 nm excitations, respectively. The inset in (c) is the bright field image of the electrospun PDLA/PLLA nanofibers. The CQDs intrinsically tended to aggregate on the nanoscale in the polymer matrix, and their aggregates range from 3–9 nm and 3–13 nm in size, respectively, for the PDLA/PLLA/CQDs with 1 wt% and 2 wt% CQD concentrations.

the hybrid nanofibers with distinct size-distributed CQD aggregates. The emission peaks were centered at 488, 563 and 706 nm for the $PDLA_{49.5}/PLLA_{49.5}/CQD_1$ nanofibers, and were centered at 522, 564 and 688 nm for the $PDLA_{49}/PLLA_{49}/CQD_2$ nanofibers when the mixtures were excited by the optimal excitation wavelengths of 405, 488 and 640 nm, respectively. Moreover, the chromaticity coordinates in the CIE diagrams (Fig. 3k and l), calculated from the $PDLA_{49.5}/PLLA_{49.5}/CQD_1$ and $PDLA_{49}/PLLA_{49}/CQD_2$ mixtures at the optimum excitations, respectively, are consistent with the LSCM and PL observations.

For one-dimensional (1D) piezoelectric materials, it is well established that the macro/nanoscale structures as well as morphologies play a key role in the enhancement of electrical signal generation.[7] The size and morphology of the electrospun polymer fibers are essentially related to the nature of the spinning solutions and spinning conditions.[43] Generally, numerous undesired pores were noticed on the electrospun PLA fibers, prepared with a spinning solvent of methylene chloride or chloroform.[43] Fig. 4 gives the SEM micrographs of the nanofibers based on PDLA, $PDLA_{50}/PLLA_{50}$ and $PDLA_{49.5}/PLLA_{49.5}/CQD_1$, respectively, electrospun with the spinning solvent mixture of dichloromethane and alcohol. It can be observed that various single or multicomponent bionanofibers, all with uniform diameters (around 800 nm) and smooth surfaces, were obtained under the same optimum spinning conditions. Moreover, with a small quantity of CQDs added, the topographical structures of the electrospun PDLA/PLLA/CQD nanofibers show no significant change when compared with those of their PDLA and PDLA/PLLA counterparts.

Fig. 5 and Table 1 show the DSC results of the as-electrospun PDLA, $PDLA_{50}/PLLA_{50}$ and $PDLA_{49.5}/PLLA_{49.5}/CQD_1$ based nanofibers. On DSC thermograms, polylactides generally show lower melting temperature peaks below 180 °C, assigned to the melting of homocrystals (hc) of optically pure PLLA or PDLA, and higher melting temperature peaks above 200 °C, assigned to the melting of sc crystallites grown in enantiomeric PLA

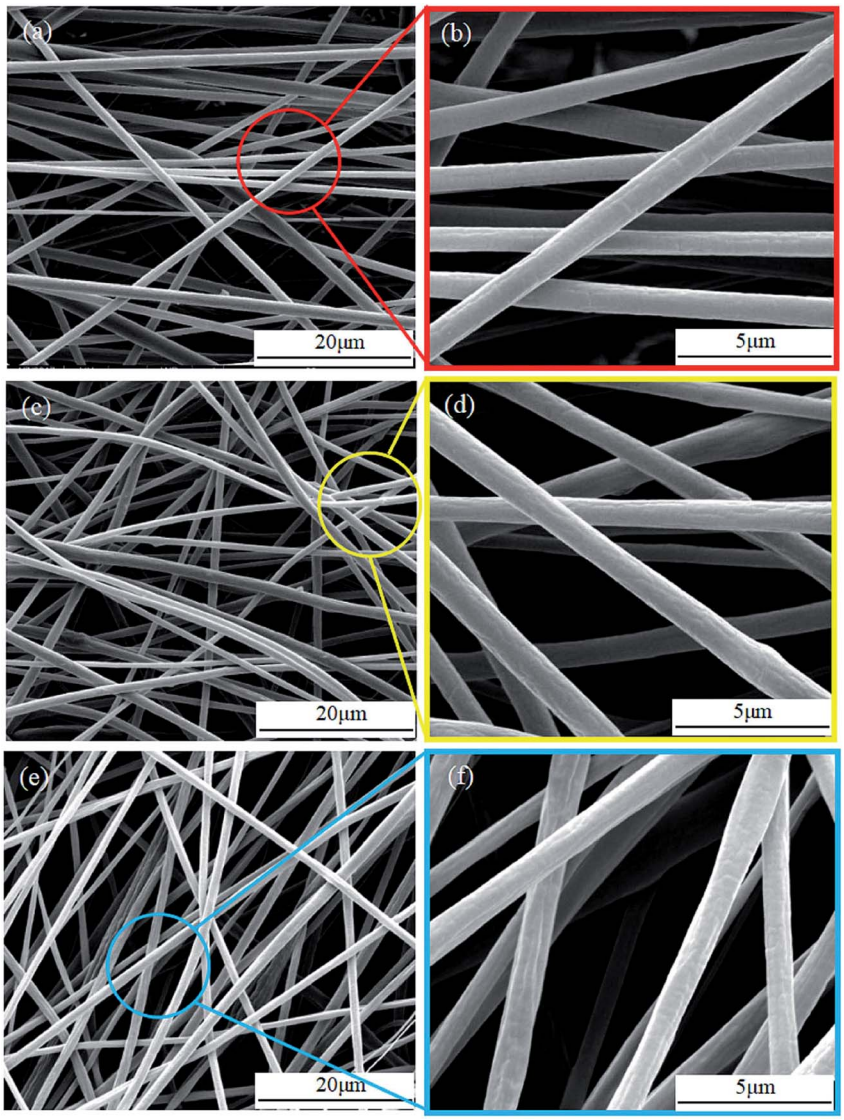


Fig. 4 SEM micrographs of the nanofibrous samples, electrospun at the applied voltage of 12 kV: (a and b) PDLA; (c and d) $PDLA_{50}/PLLA_{50}$; (e and f) $PDLA_{49.5}/PLLA_{49.5}/CQD_1$. (b), (d) and (f) are partial enlargements of (a), (c) and (e), respectively.

 

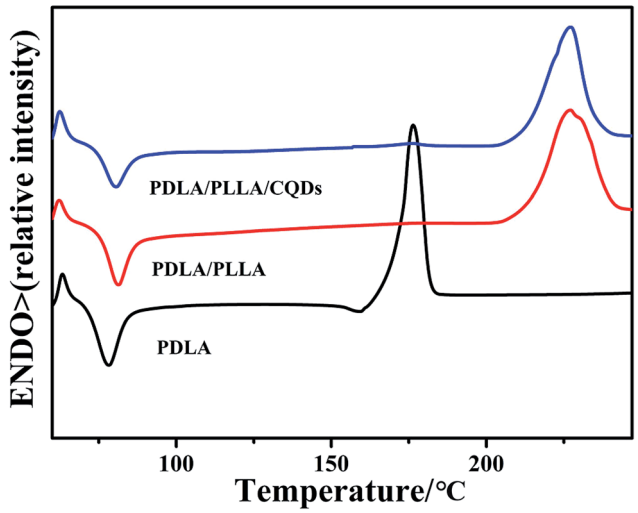


Fig. 5 DSC profiles of the PDLA, $PDLA_{50}/PLLA_{50}$ and $PDLA_{49.5}/PLLA_{49.5}/CQD_1$ based nanofibers, electrospun at the applied voltage of 12 kV.

blends.[43–48] Herein, glass transition, cold crystallization, and melting peaks are clearly observed for the electrospun PLA bionanofibers fabricated with dichloromethane and alcohol as a mixed spinning solvent. Similar to the PLA fibers electrospun with chloroform,[43] the cold crystallization peaks are adjacent to or slightly overlap with the glass transition peaks. For the PDLA fibers, the endothermic peak at 176 °C suggested that actually homocrystallites were formed. In contrast, a single endotherm, centered at 226 °C, was detected for the PDLA/PLLA/CQD nanofibers, which is the same as that of the electrospun PDLA/PLLA, confirming the co-crystallization of PLLA and PDLA in the presence of CQDs. More astonishingly, no endothermic peak corresponding to the melting of homocrystals was observed for the PDLA/PLLA/CQD nanofibers. This indicated that electrospinning at a high voltage enhanced the formation of sc crystallites, and at the same time remarkably suppressed the growth of homocrystallites in the ternary hybrid composite nanofibers. Consequently, the DSC data demonstrated that fully stereocomplexed PDLA/PLLA/CQD bionanofibers were successfully fabricated during the electrospinning process, though the sc crystallinity is somewhat slightly lower than that of their PDLA/PLLA counterparts. The formation of a stereocomplex (sc) from enantiomeric PDLA and PLLA has been proved to be an effective approach to enhance the thermal stability of the polymer.[45,46] Herein, the stereocomplexed hybrid PDLA/PLLA/CQD nanofibers have a melting point 50 °C higher than that of the PDLA based nanofibers. It is clearly evidenced that the heat resistance of the glowing bionanofibers was significantly improved through the electrospinning accelerated stereocomplexation process.

Fig. 6a schematically illustrates the charge generation process during the impact on an electrospun PDLA/PLLA/CQD hybrid nanofibrous web sample, with reference to the test results of its mechanical-to-electrical conversion (Fig. 6b–d). As shown in Fig. 6a-I, originally there is no charge on the surfaces of the bionanofiber stack. When the sample is impacted, the total thickness of the fibrous web stack decreases, resulting in an increase of the charge density on the top and bottom electrodes, due to the shear piezoelectric response of polylactides. As the compression increases, the charge density on both electrodes continues to increase. After maximum compression, the pressure starts to reduce and the sample subsequently returns to the original thickness with maximum charge density. Moving to Fig. 6a-II, the variation of charge density subsequently reaches a steady and persistent state with the continued application of impact pressure. With sample squeezing, the total thickness of the charged nanofiber stack decreases again, causing the charge density on the top and bottom electrodes to decrease. The current flows from the bottom to the top electrode, and an instantaneous positive signal output is generated. As the compression further increases, the charge density on both electrodes continues to decrease until a new equilibrium state is attained. In the releasing process, the charge density on both electrodes also increases. This results in the current flowing back from the top to bottom electrode, and a negative signal output is induced accordingly. Afterwards, the sample returns to its original state, and the cycle then repeats itself. In this way, stable and durable power generation is realized from the glowing stereocomplexed hybrid bionanofibers.

The switching polarity test is generally used to identify whether the piezoelectric signal is an artifact, resulting from the influence of the measurement system and environment, or the true electricity output, originating from the piezoelectric property of a PNG.[55–61] Herein, switching polarity tests were also conducted in order to further determine whether the electrical outputs were actually generated by the assembled bio-PNGs. Fig. 6b schematically illustrates the forward and reverse connection configurations of the PDLA/PLLA/CQD based bio-

Table 1 DSC data of the PDLA, $PDLA_{50}/PLLA_{50}$ and $PDLA_{49.5}/PLLA_{49.5}/CQD_1$ nanofibers, electrospun at the applied voltage of 12 kV

| Specimen ($x/y/z$) | $T_g$[a] (°C) | $T_{cc}$[b] (J g$^{-1}$) | $T_m$(hc)[c] (°C) | $T_m$(sc)[c] (°C) | $\Delta H_{cc}$[d] (J g$^{-1}$) | $\Delta H_m$(hc)[e] (J g$^{-1}$) | $\Delta H_m$(sc)[e] (J g$^{-1}$) | $X_c$(hc)[f] (%) | $X_c$(sc)[f] (%) |
|---|---|---|---|---|---|---|---|---|---|
| 100/0/0 | 55 | 81 | 176 | — | 22.07 | 55.82 | 0 | 31.84 | 0 |
| 50/50/0 | 55 | 82 | — | 226 | 19.49 | 0 | 74.02 | 0 | 38.40 |
| 49.5/49.5/1 | 55 | 78 | — | 226 | 24.43 | 0 | 65.23 | 0 | 29.02 |

[a] Glass transition temperature. [b] Cold crystallization temperature. [c] $T_m$(hc) and $T_m$(sc) are the melting temperatures of homocrystallites and stereocomplex crystallites, respectively. [d] Cold crystallization peak area. [e] $\Delta H_m$(hc) and $\Delta H_m$(sc) are the melting enthalpy of homocrystallites and stereocomplex crystallites, respectively. [f] $X_c$(hc) and $X_c$(sc) are the crystallinities of homocrystallites and stereocomplex crystallites, respectively, calculated from DSC measurements. The theoretical melting enthalpies of homocrystallites and stereocomplex crystallites are assumed to be 106 and 142 J g$^{-1}$, respectively.[33]

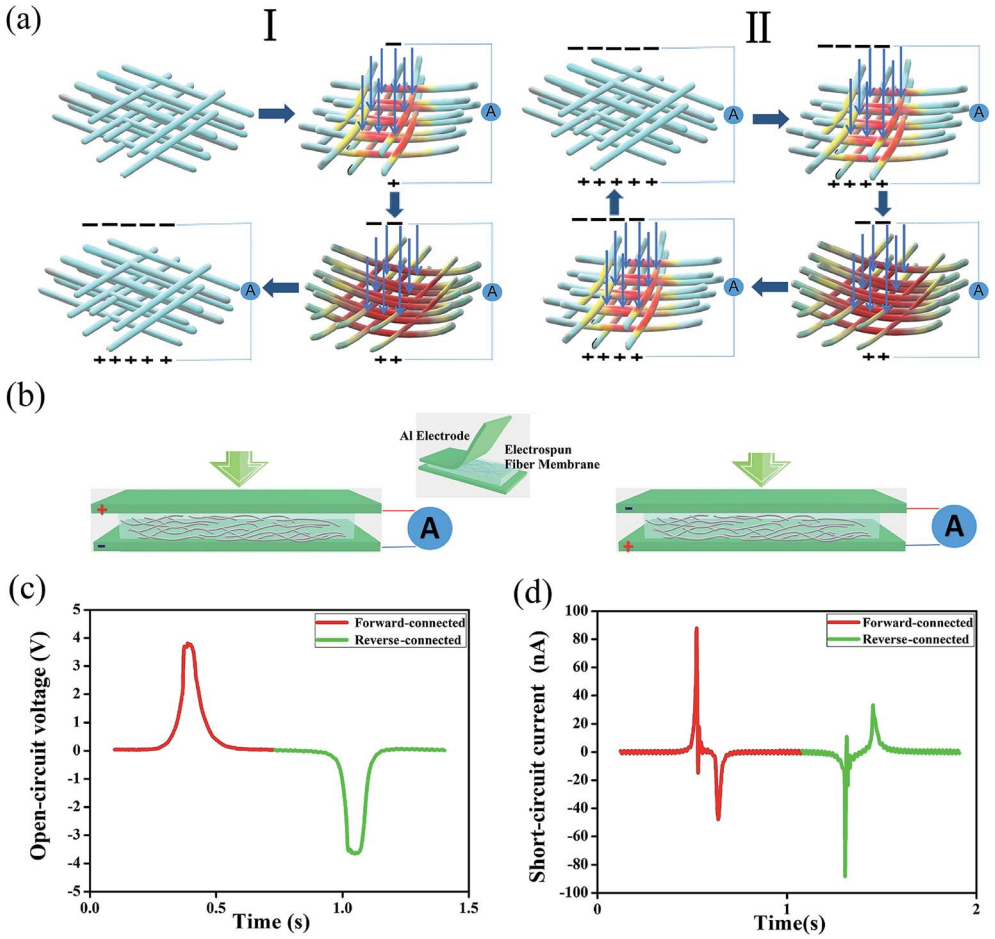


Fig. 6 Schematic drawing of the power generation process of PDLA/PLLA/CQD nanofibers (a), schematic illustration of the forward (left) and reverse (right) connection configurations of the PDLA/PLLA/CQD based bio-PNGs in reference to the measurement system (b), and the generated open-circuit voltage (c) and short-circuit current (d) of the 7-layer stacked $PDLA_{49.5}/PLLA_{49.5}/CQD_1$ nanofibrous web when it is forward- and reverse-connected to the measurement system at a stimulation frequency of 1.5 Hz and applied force of 10 N. Sample size: 2 cm × 2 cm.

PNGs under mechanical impact, in reference to the measurement system. For the forward connection test, the positive probe and negative probe of the measurement system, respectively, are connected to the positive and negative ends of a bio-PNG. In contrast, the positive and negative probes of the measurement system are respectively connected to the negative and positive ends of the same bio-PNG for the reverse connection test. The electrodes of the 7-layer stacked $PDLA_{49.5}/PLLA_{49.5}/CQD_1$ nanofiber based PNG were connected in forward and reverse connections, respectively, and the obtained open-circuit voltage output and short-circuit current signals are shown in Fig. 6c and d, respectively. As expected, the wave patterns of the forward- and reverse-connected output signals were in opposite directions. Also, there was little difference between the electrical output values. It is hence proved that the measured electrical signals are indeed piezo signals generated by the hybrid bionanofibers instead of triboelectric signals from the measurement system.

We also noted that in Fig. 6c and d the difference between the positive and negative voltage peaks is much greater than that between the current peaks. The short-circuit current signals revealed more characteristics of alternating current (AC), and the positive and negative pulses were generated, respectively, with the direct impact and the subsequent relaxed stress from the damping effect. Nevertheless, in contrast with the positive voltage peak, the negative voltage peak was almost negligible, and the voltage value appeared only as a unidirectional peak on this device. Similar electrical output results were also observed on flexible piezoelectric $(1-x)Pb(Mg_{1/3}Nb_{2/3})O_3$-$XPbTiO_3$ (PMN-PT) nanowire based nanocomposites and devices.[61] It was reported that a piezoelectric nanocomposite based nanogenerator could also serve as a capacitor.[61,62] When a piezoelectric voltage is generated, the induced charges are stored on the electrode surfaces, and will then be consumed if an opposite voltage is applied.[61] Consequently, the measured value of the negative voltage is always negligibly small if compared with that of the positive voltage.[61] Distinct from the open-circuit voltage, the induced short-circuit current mainly depends on the amplitude of the piezoelectric potential.[61] There is no significant difference between the piezoelectric potentials generated by the direct impact and the subsequent relaxed

 

stress, hence the difference between the measured values of the positive and negative currents is not so obvious.[61]

Fig. 7 shows a comparison of the electrical outputs of the 5-layer stacked 2 cm × 2 cm electrospun PDLA, $PDLA_{50}/PLLA_{50}$ and $PDLA_{49.5}/PLLA_{49.5}/CQD_1$ based nanofibrous webs, generated at a stimulation frequency of 1.5 Hz and applied force of 10 N. Generally, the optically pure polylactides have very small shear piezoelectric responses. Nevertheless, the current and voltage outputs of the as-prepared PDLA nanofibers reached 102 nA and 3.6 V, respectively, further suggesting that a relatively high degree of orientation of chiral crystallites and molecular chains was achieved during the electrospinning. More interestingly, although PDLA and PLLA have opposite signs of the piezoelectric constant, more improved piezoelectric responses were still observed on the electrospun stereocomplexed PDLA/PLLA sample. Its short-circuit current and open-circuit voltage outputs reached 125 nA and 3.8 V, respectively. This should be attributed to the favorable orientation of the C=O dipoles of the nanofibers, within and outside the stereocomplexed regions, caused by the optimum high voltage stimulation of electrospinning, together with their ideal macro/microscale topographical structures, created with the assistance of a special mixed spinning solvent. For the PDLA/PLLA/CQD nanofibers, the generated current and voltage outputs were 89.2 nA and 3.1 V, respectively. With the same heat resistance being retained, the stereocomplexed hybrid bionanofibers achieved electrical outputs comparable to those of their PDLA/PLLA counterparts. Moreover, multicolor photoluminescence was achieved, due to the successful introduction of CQDs. Therefore, a self-powered multifunctional bionanofiber is realized with the electrospinning technique and may present new potentials in a new generation of autonomous optoelectronic devices.

Compared with those of the PDLA/PLLA nanofibers, the electrical outputs of the PDLA/PLLA/CQD nanofibers were slightly reduced (Fig. 7). Nevertheless, the introduction of CQDs enabled the hybridized nanofibers to emit the desired excitation-light dependent multicolor luminescence (Fig. 3). Also, the PDLA/PLLA composite materials showed better heat resistance than pure PDLA or PLLA, due mainly to the formation of stereocomplexed crystals (Fig. 5 and Table 1). Further studies using electrospun PDLA/PLLA/CQD nanofibrous films as piezoelectric units showed that their piezoelectric outputs might be optimized with the flexible stacking of collapsible nanowebs as well as the tuning of the amplitude and/or frequency of stimulated dynamic loads. Thus, the combined advantages of high piezoresponse, multicolor luminescence and simultaneously improved heat resistance could be achieved in a single PDLA/PLLA/CQD based composite, allowing the development of a new mechatronics platform for multifunctional self-powered bio-devices.

Fig. 8 shows the generated voltage and current outputs of the increasingly layered electrospun $PDLA_{49.5}/PLLA_{49.5}/CQD_1$ nanoweb stacks, at a stimulation frequency of 1.5 Hz and applied force of 10 N. Both the open-circuit voltages and short-circuit currents increased with the increase of the stacked layers of PDLA/PLLA/CQD nanowebs. At the maximum of 7 layers, the short-circuit current and the corresponding open-circuit voltage reached 103 nA and 3.8 V, respectively. According to a calculation, the voltage output density of the 7-layer stacked PDLA/PLLA/CQD nanoweb is 29.69 V $cm^{-3}$. It can be seen that if the number of layers is continuously increased, the generated electrical outputs will continue to increase accordingly.

Comparisons of electrical outputs were made with other processed PDLA/PLLA/CQD materials. Fig. S2, ESI† shows the electrical outputs of the $PDLA_{49.5}/PLLA_{49.5}/CQD_1$ based films, fabricated through direct solution casting and electrospinning at 0 and 1400 rpm rotating speed, respectively. For the solution cast PDLA/PLLA/CQD film, very low current and voltage outputs were observed at a stimulation frequency of 1.5 Hz and applied force of 10 N. Nevertheless, the electrical outputs of PDLA/PLLA/CQDs were improved remarkably by the electrospinning process, due mainly to the electrospinning enhanced orientation of chiral crystallites and molecular chains. Moreover, the electrical outputs of the electrospun PDLA/PLLA/CQD nanofibrous films increased with an increase in the rotation speed of the receiving device, as the speed increase of the rotating drum may further increase the orientation degree of the chiral crystallites and molecular chains of the nanofibers. Herein, the PDLA/PLLA/CQD nanofibrous films electrospun at 0 and 1400

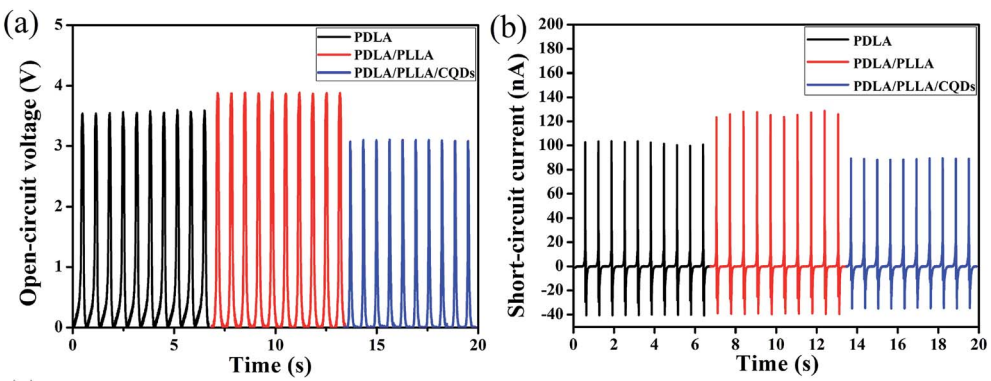


Fig. 7 Open-circuit voltage (a) and short-circuit current (b) outputs of the electrospun PDLA, $PDLA_{50}/PLLA_{50}$ and $PDLA_{49.5}/PLLA_{49.5}/CQD_1$ based nanofibrous web stacks with 5 layers, generated at a stimulation frequency of 1.5 Hz and applied force of 10 N. The size is 2 cm × 2 cm for each sample.

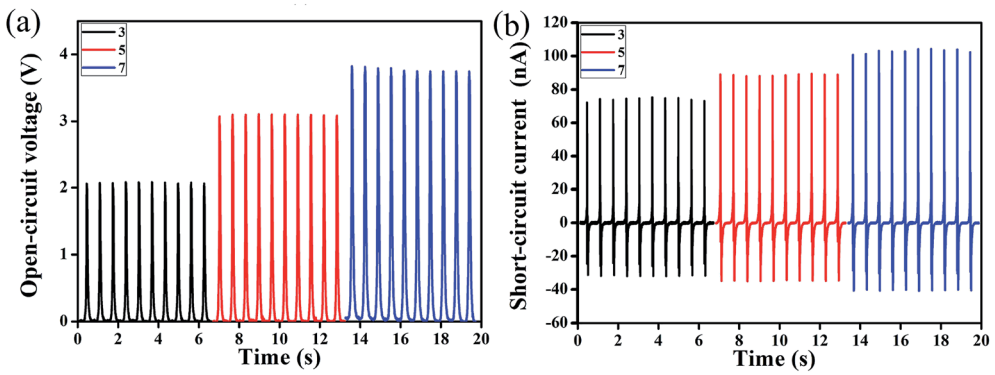


Fig. 8 Open-circuit voltage (c) and short-circuit current (d) outputs of the electrospun $PDLA_{49.5}/PLLA_{49.5}/CQD_1$ nanoweb stacks, with an increasing number of layers, generated at a stimulation frequency of 1.5 Hz and applied force of 10 N. The size is 2 cm × 2 cm for each sample.

rpm rotating speeds are termed unoriented and oriented electrospun films, respectively. The short-circuit current output of the oriented electrospun film exceeded that of the unoriented electrospun film by four times, while the open-circuit voltage output was two times higher than that of the unoriented electrospun film.

The piezoelectric electrical outputs of PDLA/PLLA/CQD nanofibers were also investigated with the changes in electrospinning voltage as well as in the PDLA/PLLA ratio. Fig. S3, ESI† shows the electrical outputs of the $PDLA_{49.5}/PLLA_{49.5}/CQD_1$ nanofibrous films electrospun at various spinning voltages, generated at a stimulation frequency of 1.5 Hz and applied force of 10 N. With the increase of the spinning voltage from 9 to 16 kV, the open-circuit voltage output increased slightly, whereas the optimum short-circuit current output was observed at 12 kV, and was much higher than that at 9 or 16 kV. The electrical outputs showed the same trend with the increase in the PDLA/PLLA ratio in the electrospun PDLA/PLLA/CQD nanofibrous films (Fig. S4, ESI†). Although the generated open-circuit voltage increased with the increase in PDLA content, the highest short-circuit current was achieved with a PDLA/PLLA/CQD nanofibrous film in which the PDLA and PLLA were mixed in the same ratio. The phenomena in which the current and voltage output variations do not always show the same trend were also observed in other kinds of PNGs with the utilization of 1D polymer nanofibers.[58] The above results suggested that the PDLA/PLLA/CQD based hybrid bionanofibers with optimal electrical output were able to be fabricated by tuning the electrospinning conditions as well as the internal composite structures.

To put these kinds of hybrid bionanofibers into practical use, it is necessary to consider the diversification of the external dynamic stimulus, as the frequency and intensity of the applied impact in real situations may not be as regular as those in the laboratory. Therefore, the mechanical-to-electrical conversions of a 7-layer $PDLA_{49.5}/PLLA_{49.5}/CQD_1$ nanofibrous web stack sample, with an area of 2 cm × 2 cm and a volume of 0.128 $cm^3$, were evaluated by controlling the frequency and amplitude of the stimulation force, and the generated voltage and current outputs are shown in Fig. 9. With the increase of stimulation frequency at a given force of 10 N, both the open-circuit voltage and short-circuit current outputs increased significantly (Fig. 9a and b). When the frequency increased from 1.5 to 3 Hz, the voltage outputs increased step by step from 3.8 to 9.5 V. At the same time, the short-circuit current was accordingly raised to 620 nA. We also noted that a huge rise in current output occurred when the frequency was increased above 2 Hz. Comparing the current results generated at 2 and 2.5 Hz, the short-circuit current increased exponentially from 158 to 480 nA. The maximum electrical output values were observed at 3 Hz, with an open-circuit voltage output density of 74.2 V $cm^{-3}$ and a short-circuit current output density of 4.9 μA $cm^{-3}$. The electrical output increase with the variation of the applied frequency was also evidenced in poly(vinylidene fluoride) or poly(vinylidenefluoride-*co*-trifluoroethylene) based piezoelectric nanogenerators as well as in cellular polypropylene piezoelectric generators.[58–60] For a PNG utilizing an elastic piezopolymer, its dynamic modulus increases with the increase of stimulation frequency, and this in turn results in an increased output response at higher frequencies.[58] Also, the strain rate of the PNG increases when the loading frequency increases with a fixed strain magnitude.[59] In such cases, more bound charges are generated, consequently leading to larger piezoelectric voltage and current.[59]

Moreover, the short-circuit current as well as the corresponding open circuit voltage produced by the press-and-release cycles increased when the magnitude of the stimulation force was increased at a fixed frequency of 1.5 Hz (Fig. 9c and d). With a force from 10 to 200 N, the voltage increased from 3.8 to 7.9 V, corresponding to a maximum density of 61.7 V $cm^{-3}$, and the current also increased from 113 to 313 nA, corresponding to a maximum density of 2.5 μA $cm^{-3}$. According to the above results, increasing the magnitude and frequency of the excitation force can lead to a larger electrical output for the soft electrospun hybrid bionanofibers, but the increase is not infinite. Excessive excitation and frequency may damage the fibrous samples. Also, the increase of the electrical output of the hybridized stereocomplex nanofibers is more sensitive to the variation of stimulation frequency. A very high electrical output density can be realized with a relatively lower magnitude of dynamic load at a higher frequency.

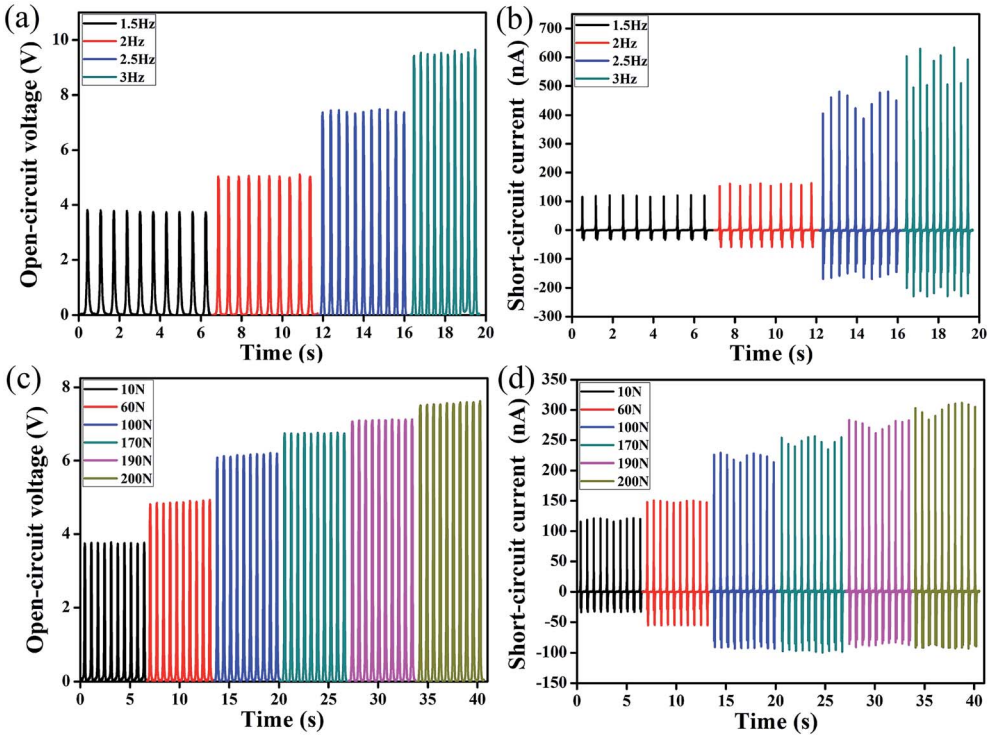


Fig. 9 Electrical outputs of the electrospun $PDLA_{49.5}/PLLA_{49.5}/CQD_1$ nanofibrous web stacks with 7 layers under various loads or frequencies: (a) open-circuit voltage and (b) short-circuit current outputs, stimulated at different frequencies and a given force of 10 N; (c) open-circuit voltage and (d) short-circuit current outputs, stimulated at different forces and a fixed frequency of 1.5 Hz. Sample size: 2 cm × 2 cm.

To determine the optimum electrical output power, the output voltage and current of the electrospun nanofibrous PDLA/PLLA/CQDs were further measured under various external load resistances. As shown in Fig. 10a, with the increase of the external resistance, the short-circuit current amplitude decreased, due mainly to the ohmic loss, whereas the open-circuit voltage followed a reverse trend. The change was particularly sharp when the load resistance was increased from 10 MΩ to 1 GΩ. The dependence of the calculated instantaneous peak power density on load resistance is plotted in Fig. 10b for a 7-layer $PDLA_{49.5}/PLLA_{49.5}/CQD_1$ nanofibrous web stack sample stimulated at 1.5 Hz and 10 N. The instantaneous peak power was maximized at an external load resistance of 384 MΩ, corresponding to a peak power density of 5.5 μW $cm^{-3}$.

For the electrospun nanofibrous PDLA/PLLA/CQDs, high piezoelectric outputs have been obtained by tuning the amplitude and/or frequency of the stimulated dynamic force. However, it is still necessary to further study whether the hybrid bionanofibers are able to output the piezoelectric signals for a long period of time, as long-term stable and durable energy harvesting is vital to the operation of a sustainable and autonomous bioelectronic device. Herein, short-circuit current output is chosen as the main parameter in evaluating the stability and durability of the PDLA/PLLA/CQD nanofiber based PNG. At a force of 10 N and a frequency of 1.5 Hz, the 7-layer $PDLA_{49.5}/PLLA_{49.5}/CQD_1$ nanoweb stack was impacted for about 10 000 cycles, and the corresponding current output is shown in Fig. 11a. More interestingly, not only did no performance degradation happen for the sample during the test cycles, but the current output also increased in the initial stage. With the increase of experimental time, the output of the short-circuit current kept increasing under the continuous impact until the hits reached 5000 cycles, and then it became stable and repeatable, with a maximum value of 145 nA. This means the piezoelectric outputs of the bio-PNG will not attenuate over a long period of dynamic load, and more kinetic energy can be collected instead due mainly to a self-perfection of the electrospun fibrous web under the sustained impact. The self-improvement of the electrical output performance may be attributed to the unique internal composite structure of the bio-PNG. The electrospun nanofiber web is similar to a cotton-like textile fabric, and the inside is a porous and soft structure arranged with countless filaments. The fluffy nanofiber webs are continuously compacted during long term impact, and more charges are hence accumulated on the bio-PNG electrodes, corresponding to the increasing electrical outputs in the early stage. Nevertheless, with the impact cycles further increasing, a balance state is achieved between the stress and relaxation of the nanofibrous webs, and then they achieve stabilized but improved piezoelectric outputs. During the stability and durability test, a LED was connected to the electrodes at both ends of the 2 cm × 2 cm hybridized nanofibrous bio-PNG, and the light bulb kept shining with the cyclical impacts on the sample, as shown in Fig. 11b. In view of the results, it is conceivable that more stable electrical power will be generated by using a larger amount of such fiber web stacks for the assembling of bio-PNGs. This signifies the great potential of the electrospun hybrid bionanofibers in many commercial applications.

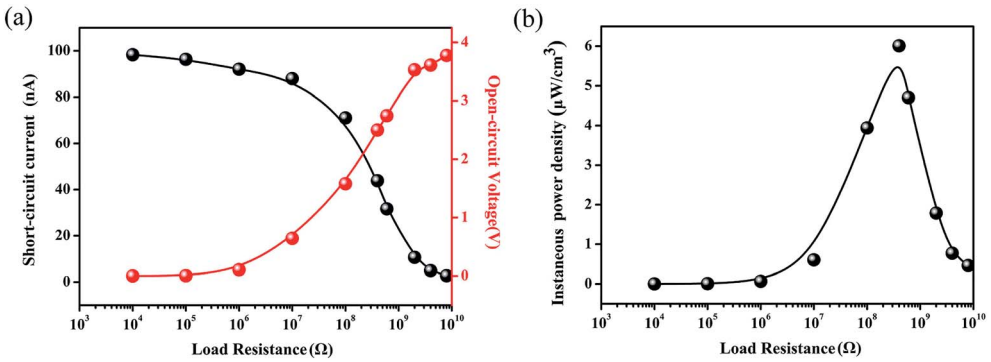


Fig. 10 Dependence of the voltage and current outputs (a) and the calculated power density (b) on external load resistance, for a 7-layer $PDLA_{49.5}/PLLA_{49.5}/CQD_1$ nanofibrous web stack sample, stimulated at 1.5 Hz and 10 N. The points represent peak values of the electrical signals, and the curves are fitted results. Sample size: 2 cm × 2 cm.

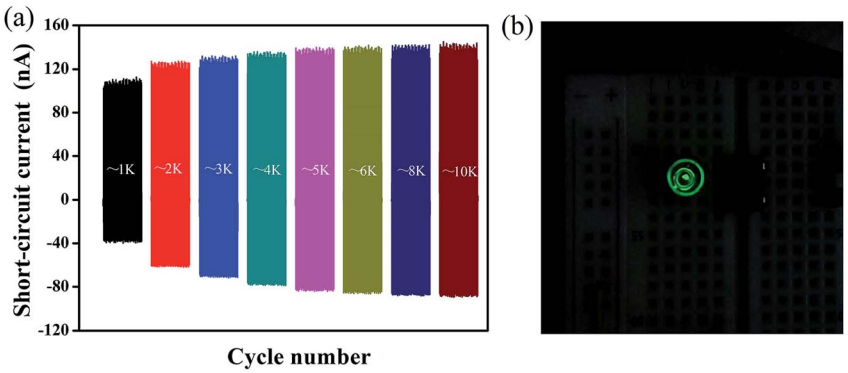


Fig. 11 Output current–time curves of the 7-layer $PDLA_{49.5}/PLLA_{49.5}/CQD_1$ nanoweb stack for ≈10 000 continuous working cycles, whole signal, stimulated by a 1.5 Hz and 10 N impact (a), and a digital picture showing the LED operated with the generated power during the stability and durability test (b). Sample size: 2 cm × 2 cm.

## Conclusion

In summary, we have demonstrated the successful design and fabrication of a novel electrospun stereocomplex PDLA/PLLA/CQD based hybrid nanofiber. The introduction of CQDs during electrospinning endowed the hybridized bionanofibers with desirable excitation-light dependent multicolor luminescence. Also, the optimum high voltage stimulation of electrospinning, with the assistance of mixed dichloromethane and alcohol as a spinning solvent, favored the manufacture of PDLA/PLLA/CQD nanofibers with ideal macro/microscale topographical structures, and remarkably enhanced the formation and orientation of the internal stereocomplexed crystallites. This, in turn, allowed the luminous fibers to harvest dynamic mechanical energy with a direct piezoelectric conversion of high efficiency. Being assembled as a bio-PNG, the electrical outputs of the electrospun stereocomplex bionanofibers were optimized with the flexible stacking of collapsible nanowebs as well as the tuning of the amplitude and/or frequency of stimulated dynamic loads, and the maximum open-circuit voltage and short-circuit current output density achieved were 74.2 V $cm^{-3}$ and 4.9 μA $cm^{-3}$, respectively. As a power source to operate LEDs, the stereocomplexed hybrid bio-PNG showed good stability and durability together with a self-perfection mechanism, and no decay in electrical output was observed for more than 10 000 continuous working cycles. Considering their combined advantages of high shear piezoresponse, multicolor photoluminescence and simultaneously improved heat resistance, the as-developed multifunctional hybrid bionanofibers may have promising applications in environmentally friendly self-powered bio-sensors and bio-piezoelectric nanogenerators in a new-generation of transient electronics and implantable medical devices.

## Author contributions

Jun Lu conceived the idea and initiated the study. Yali Xu, Long Jin, Xuebing He, Xi Huang, Meilin Xie, Chuanfeng Wang and Chaoliang Zhang carried out the sample preparation and characterization. Jun Lu, Weiqing Yang and Fanbin Meng organized the entire research. Yali Xu, Jun Lu, Long Jin, Weiqing Yang and Fanbin Meng analysed and interpreted the data, and wrote the manuscript with the assistance of all the other co-authors. All the authors discussed the results and commented on the manuscript.

## Competing financial interests

The authors declare no competing financial interest.

## Conflicts of interest

There are no conflicts to declare.

## Acknowledgements

This work was financially supported by the Sichuan Science and Technology Program (No. 2018JY0166) and the Opening Project of State Key Laboratory of Polymer Materials and Engineering (Sichuan University) (No. sklpme2017-4-03). The authors extend their gratitude to Professor Yajiang Huang (Sichuan University) for valuable discussions.

## References

1 Y. Q. Zhu, C. Romain and C. K. Williams, Sustainable polymers from renewable resources, *Nature*, 2016, **540**, 354–362.
2 H. J. Kim, J. H. Kim, K. W. Jun, J. H. Kim, W. C. Seung, O. H. Kwon, J. Y. Park, S. W. Kim and I. K. Oh, Silk nanofiber-networked bio-triboelectric generator: silk bio-TEG, *Adv. Energy Mater.*, 2016, **6**, 1502329.
3 Y. K. Bao, R. X. Wang, Y. M. Lu and W. Z. Wu, Lignin biopolymer based triboelectric nanogenerators, *APL Mater.*, 2017, **5**, 074109.
4 E. N. Jayaweera, K. R. Wijewardhana, T. K. Ekanayaka, A. Shahzad and J. K. Song, Triboelectric nanogenerator based on human hair, *ACS Sustainable Chem. Eng.*, 2018, **6**, 6321–6327.
5 R. X. Wang, S. J. Gao, Z. Yang, Y. L. Li, W. N. Chen, B. X. Wu and W. Z. Wu, Engineered and laser-processed chitosan biopolymers for sustainable and biodegradable triboelectric power generation, *Adv. Mater.*, 2018, **30**, 1706267.
6 W. Jiang, H. Li, Z. Liu, Z. Li, J. J. Tian, B. J. Shi, Y. Zou, H. Ouyang, C. C. Zhao, L. M. Zhao, R. Sun, H. R. Zheng, Y. B. Fan, Z. L. Wang and Z. Li, Fully bioabsorbable natural-materials-based triboelectric nanogenerators, *Adv. Mater.*, 2018, **30**, 1801895.
7 Z. L. Wang and J. Song, Piezoelectric nanogenerators based on zinc oxide nanowire arrays, *Science*, 2006, **163**, 242–246.
8 C. W. Xu, L. Zhang, Y. L. Xu, Z. Z. Yin, Q. Chen, S. Y. Ma, H. H. Zhang, R. Huang, C. L. Zhang, L. Jin, W. Q. Yang and J. Lu, Filling the holes in piezopolymers with a solid electrolyte: a new paradigm of poling-free dynamic electrets for energy harvesting, *J. Mater. Chem. A*, 2017, **5**, 189–200.
9 S. K. Ghosh and D. Mandal, High-performance bio-piezoelectric nanogenerator made with fish scale, *Appl. Phys. Lett.*, 2016, **109**, 103701.
10 S. K. Ghosh and D. Mandal, Efficient natural piezoelectric nanogenerator: electricity generation from fish swim bladder, *Nano Energy*, 2016, **28**, 356–365.
11 K. L. Ren, W. L. Wilson, J. E. West, Q. M. Zhang and S. M. Yu, Piezoelectric property of hot pressed electrospun poly(γ-benzyl-α,L-glutamate) fibers, *Appl. Phys. A*, 2012, **107**, 639–646.
12 K. Tanimoto, S. Saihara, Y. Adachi, Y. Harada, Y. Shiomi and Y. Tajitsu, Shear piezoelectricity of optically active polysuccinimides, *Jpn. J. Appl. Phys.*, 2015, **54**, 10NF02.
13 Q. Y. Pan, S. Tasaka, O. Furutani and N. Inagaki, Ferroelectric and pyroelectric behaviors in poly(glycolic acid), *Polym. J.*, 1999, **31**, 903–907.
14 T. Putzeys and M. Wübbenhorst, Polarization domain information on insect wing chitin using the scanning pyroelectric microscope (SPEM), *IEEE Trans. Dielectr. Electr. Insul.*, 2015, **22**, 1394–1400.
15 A. Heredia, V. Meunier, I. K. Bdikin, J. Gracio, N. Balke, S. Jesse, A. Tselev, P. K. Agarwal, B. G. Sumpter, S. V. Kalinin and A. L. Kholkin, Nanoscale ferroelectricity in crystalline γ-glycine, *Adv. Funct. Mater.*, 2012, **22**, 2996–3003.
16 E. Fukada, Poiseuille medal award lecture: piezoelectricity of biopolymers, *Biorheology*, 1995, **32**, 593–609.
17 T. Yucel, P. Cebe and D. L. Kaplan, Structural origins of silk piezoelectricity, *Adv. Funct. Mater.*, 2011, **21**, 779–785.
18 T. Li and K. Y. Zeng, Nano-hierarchical structure and electromechanical coupling properties of clamshell, *J. Struct. Biol.*, 2012, **180**, 73–83.
19 T. Li and K. Y. Zeng, Nanoscale piezoelectric and ferroelectric behaviors of seashell by piezoresponse force microscopy, *J. Appl. Phys.*, 2013, **113**, 187202.
20 X. L. Zhou, H. C. Miao and F. X. Li, Nanoscale structural and functional mapping of nacre by scanning probe microscopy techniques, *Nanoscale*, 2013, **5**, 11885–11893.
21 V. Nguyen, K. Jenkins and R. S. Yang, Epitaxial growth of vertically aligned piezoelectric diphenylalanine peptide microrods with uniform polarization, *Nano Energy*, 2015, **17**, 323–329.
22 Z. Zhou, D. Qian and M. Minary-Jolandan, Molecular mechanism of polarization and piezoelectric effect in super-twisted collagen, *ACS Sustainable Chem. Eng.*, 2016, **2**, 929–936.
23 S. Guerin, A. Stapleton, D. Chovan, R. Mouras, M. Gleeson, C. McKeown, M. R. Noor, C. Silien, F. M. F. Rhen, A. L. Kholkin, N. Liu, T. Soulimane, S. A. M. Tofail and D. Thompson, Control of piezoelectricity in amino acids by supramolecular packing, *Nat. Mater.*, 2018, **17**, 180–186.
24 X. H. Zou and G. Q. Chen, Metabolic engineering for microbial production and applications of copolyesters consisting of 3-hydroxybutyrate and medium-chain-length 3-hydroxyalkanoates, *Macromol. Biosci.*, 2007, **7**, 174–182.
25 C. S. Lovell, J. H. Kang, G. Sauti, J. M. Fitz-Gerald and C. Park, Shear piezoelectricity in single-wall carbon nanotube/poly(γ-benzyl-L-glutamate) composites, *J. Polym. Sci., Part B: Polym. Phys.*, 2010, **48**, 2355–2365.
26 C. S. Lovell, J. M. Fitz-Gerald and C. Park, Decoupling the effects of crystallinity and orientation on the shear piezoelectricity of polylactic acid, *J. Polym. Sci., Part B: Polym. Phys.*, 2011, **49**, 1555–1562.

27 M. Smith, Y. Calahorra, Q. S. Jing and S. Kar-Narayan, Direct observation of shear piezoelectricity in poly-L-lactic acid nanowires, *APL Mater.*, 2017, **5**, 074105.
28 E. J. Curry, K. Ke, M. T. Chorsi, K. S. Wrobel, A. N. Miller, A. Patel, I. Kim, J. L. Feng, L. X. Yue, Q. Wu, C. L. Kuo, K. W. H. Lo, C. T. Laurencin, H. Ilies, P. K. Purohit and T. D. Nguyen, Biodegradable piezoelectric force sensor, *Proc. Natl. Acad. Sci. U. S. A.*, 2018, **115**, 909–914.
29 J. Morvan, E. Buyuktanir, J. L. West and A. Jákli, Highly piezoelectric biocompatible and soft composite fibers, *Appl. Phys. Lett.*, 2012, **100**, 063901.
30 M. Varga, J. Morvan, N. Diorio, E. Buyuktanir, J. Harden, J. L. West and A. Jákli, Direct piezoelectric responses of soft composite fiber mats, *Appl. Phys. Lett.*, 2013, **102**, 153903.
31 K. May, A. Eremin, R. Stannarius, S. Klein, K. Neyts, J. Harden and A. Jákli, Piezoelectric fiber mats containing polar rod-shaped pigment particles, *RSC Adv.*, 2014, **4**, 44223–44228.
32 D. da Silva, M. Kaduri, M. Poley, O. Adir, N. Krinsky, J. Shainsky-Roitman and A. Schroeder, Biocompatibility, biodegradation and excretion of polylactic acid (PLA) in medical implants and theranostic systems, *Chem. Eng. J.*, 2018, **340**, 9–14.
33 J. R. Sarasua, A. L. Arraiza, P. Balerdi and I. Maiza, Crystallinity and mechanical properties of optically pure polylactides and their blends, *Polym. Eng. Sci.*, 2005, **45**, 745–753.
34 G. M. Liu, X. Q. Zhang and D. J. Wang, Tailoring crystallization: towards high-performance poly(lactic acid), *Adv. Mater.*, 2014, **26**, 6905–6911.
35 E. Fukada, History and recent progress in piezoelectric polymers, *IEEE Trans. Ultrason. Ferroelectr. Freq. Control.*, 2000, **47**, 1277–1290.
36 M. Smyth, V. Poursorkhabi, A. K. Mohanty, S. Gregori and M. Misra, Electrospinning highly oriented and crystalline poly(lactic acid) fiber mats, *J. Mater. Sci.*, 2014, **49**, 2430–2441.
37 S. J. Lee, A. A. Prabu and K. J. Kim, Piezoelectric properties of electrospun poly(L-lactic acid) nanofiber web, *Mater. Lett.*, 2015, **148**, 58–62.
38 T. Nakiri, M. Okuno, N. Maki, M. Kanasaki, Y. Morimoto, S. Okamoto, M. Ishizuka, K. Fukuda, T. Takaki and Y. Tajitsu, Piezoelectric characteristics of chiral polymer composite films obtained under strong magnetic field, *Jpn. J. Appl. Phys.*, 2005, **44**, 7119–7122.
39 M. Yoshida, T. Onogi, K. Onishi, T. Inagaki and Y. Tajitsu, High piezoelectric performance of poly(lactic acid) film manufactured by solid-state extrusion, *Jpn. J. Appl. Phys.*, 2014, **53**, 09PC02.
40 M. G. McKee, J. M. Layman, M. P. Cashion and T. E. Long, Phospholipid nonwoven electrospun membranes, *Science*, 2006, **311**, 353–355.
41 L. Persano, A. Camposeo and D. Pisignano, Active polymer nanofibers for photonics, electronics, energy generation and micromechanics, *Prog. Polym. Sci.*, 2015, **43**, 48–95.
42 G. Yang, X. L. Li, Y. He, J. K. Ma, G. L. Ni and S. B. Zhou, From nano to micro to macro: electrospun hierarchically structured polymeric fibers for biomedical applications, *Prog. Polym. Sci.*, 2018, **81**, 80–113.
43 H. Tsuji, M. Nakano, M. Hashimoto, K. Takashima, S. Katsura and A. Mizuno, Electrospinning of poly(lactic acid) stereocomplex nanofibers, *Biomacromolecules*, 2006, **7**, 3316–3320.
44 L. Sun, A. Pitto-Barry, N. Kirby, T. L. Schiller, A. M. Sanchez, M. A. Dyson, J. Sloan, N. R. Wilson, R. K. O'Reilly and A. P. Dove, Structural reorganization of cylindrical nanoparticles triggered by polylactide stereocomplexation, *Nat. Commun.*, 2014, **5**, 5746.
45 B. H. Tan, J. K. Muiruri, Z. B. Li and C. B. He, Recent progress in using stereocomplexation for enhancement of thermal and mechanical property of polylactide, *ACS Sustainable Chem. Eng.*, 2016, **4**, 5370–5391.
46 Y. H. Jing, C. Y. Quan, B. Liu, Q. Jiang and C. Zhang, A mini review on the functional biomaterials based on poly(lactic acid) stereocomplex, *Polym. Rev.*, 2016, **56**, 262–286.
47 G. W. Pan, H. L. Xu, B. N. Mu, B. M. Ma, J. Yang and Y. Q. Yang, Complete stereo-complexation of enantiomeric polylactides for scalable continuous production, *Chem. Eng. J.*, 2017, **328**, 759–767.
48 Y. Zhong, T. T. Li, H. B. Lin, L. Zhang, Z. Xiong, Q. L. Fang, G. Y. Zhang and F. Liu, Meso-/macro-porous microspheres confining Au nanoparticles based on PDLA/PLLA stereo-complex membrane for continuous flowing catalysis and separation, *Chem. Eng. J.*, 2018, **344**, 299–310.
49 S. J. Zhu, Y. B. Song, X. H. Zhao, J. R. Shao, J. H. Zhang and B. Yang, The photoluminescence mechanism in carbon dots (graphene quantum dots, carbon nanodots, and polymer dots): current state and future perspective, *Nano Res.*, 2015, **8**, 355–381.
50 X. T. Zheng, A. Ananthanarayanan, K. Q. Luo and P. Chen, Glowing graphene quantum dots and carbon dots: properties, syntheses, and biological applications, *Small*, 2015, **11**, 1620–1636.
51 R. Wang, K. Q. Lu, Z. R. Tang and Y. J. Xu, Recent progress in carbon quantum dots: synthesis, properties and applications in photocatalysis, *J. Mater. Chem. A*, 2017, **5**, 3717–3734.
52 X. Y. Zhang, C. Y. Liu, Z. Q. Li, J. X. Guo, L. Shen, W. B. Guo, L. Zhang, S. P. Ruan and Y. B. Long, An easily prepared carbon quantum dots and employment for inverted organic photovoltaic devices, *Chem. Eng. J.*, 2017, **315**, 621–629.
53 J. L. He, Y. L. He, Y. H. Chen, X. J. Zhang, C. F. Hu, J. L. Zhuang, B. F. Lei and Y. L. Liu, Construction and multifunctional applications of carbon dots/PVA nanofibers with phosphorescence and thermally activated delayed fluorescence, *Chem. Eng. J.*, 2018, **347**, 505–513.
54 W. S. Zou, Q. C. Zhao, W. L. Kong, X. F. Wang, X. M. Chen, J. Zhang and Y. Q. Wang, Multi-level fluorescent logic gate based on polyamine coated carbon dots capable of responding to four stimuli, *Chem. Eng. J.*, 2018, **337**, 471–479.

 

55 R. S. Yang, Y. Qin, C. Li, L. M. Dai and Z. L. Wang, Characteristics of output voltage and current of integrated nanogenerators, *Appl. Phys. Lett.*, 2009, **94**, 022905.
56 Y. K. Fuh, J. C. Ye, P. C. Chen, H. C. Ho and Z. M. Huang, Hybrid energy harvester consisting of piezoelectric fibers with largely enhanced 20 V for wearable and muscle-driven applications, *ACS Appl. Mater. Interfaces*, 2015, **7**, 16923–16931.
57 V. Vivekananthan, N. R. Alluri, Y. Purusothaman, A. Chandrasekhar and S. J. Kim, A flexible, planar energy harvesting device for scavenging road side waste mechanical energy *via* the synergistic piezoelectric response of $K_{0.5}Na_{0.5}NbO_3$-$BaTiO_3$/PVDF composite films, *Nanoscale*, 2017, **9**, 15122–15130.
58 S. K. Ghosh and D. Mandal, Synergistically enhanced piezoelectric output in highly aligned 1D polymer nanofibers integrated all-fiber nanogenerator for wearable nano-tactile sensor, *Nano Energy*, 2018, **53**, 245–257.
59 Z. Y. Pi, J. W. Zhang, C. Y. Wen, Z. B. Zhang and D. P. Wu, Flexible piezoelectric nanogenerator made of poly(vinylidenefluoride-*co*-trifluoroethylene) (PVDF-TrFE) thin film, *Nano Energy*, 2014, **7**, 33–41.
60 N. Wu, X. F. Chen, Q. Z. Zhong, J. W. Zhong, W. B. Li, B. Wang, B. Hu and J. Zhou, Cellular polypropylene piezoelectret for human body energy harvesting and health monitoring, *Adv. Funct. Mater.*, 2015, **25**, 4788–4794.
61 S. Y. Xu, Y. W. Yeh, G. Poirier, M. C. McAlpine, R. A. Register and N. Yao, Flexible piezoelectric PMN-PT nanowire-based nanocomposite and device, *Nano Lett.*, 2013, **13**, 2393–2398.
62 C. Lu, L. Zhang, C. W. Xu, Z. Z. Yin, S. B. Zhou, J. X. Wang, R. Huang, X. Q. Zhou, C. L. Zhang, W. Q. Yang and J. Lu, Self-powered graphene quantum dot/poly(vinylidene fluoride) composites with remarkably enhanced mechanical-to-electrical conversion, *RSC Adv.*, 2016, **6**, 67400–67408.